Discrete-event simulation of neutron interferometry experiments

H. De Raedt, F. Jin, and K. Michielsen

Citation: AIP Conf. Proc. **1508**, 172 (2012); doi: 10.1063/1.4773129
View online: http://dx.doi.org/10.1063/1.4773129
View Table of Contents: http://proceedings.aip.org/dbt/dbt.jsp?KEY=APCPCS&Volume=1508&Issue=1
Published by the American Institute of Physics.

Discrete-event simulation of neutron interferometry experiments [1]

H. De Raedt[*], F. Jin[†] and K. Michielsen[†,**]

[*]*Department of Applied Physics, Zernike Institute for Advanced Materials, University of Groningen, Nijenborgh 4, NL-9747 AG Groningen, The Netherlands*
[†]*Institute for Advanced Simulation, Jülich Supercomputing Centre, Research Centre Jülich, D-52425 Jülich, Germany*
[**]*RWTH Aachen University, D-52056 Aachen, Germany*

Abstract. A discrete-event simulation approach that does not require the knowledge of the solution of a wave equation of the whole system, yet reproduces the statistical distributions of quantum theory by generating detection events one-by-one is illustrated by applications to single-neutron interferometry experiments, including one that shows violations of a Bell inequality.

Keywords: Neutron interference experiments, Bell inequality test, quantum theory, discrete event simulation
PACS: 03.65.Ud, 03.65.-w, 02.70.-c

INTRODUCTION

Quantum theory has proven to be extraordinarily successful in describing the spectra of atoms and molecules, the properties of solids etc. In principle, it is straightforward to start from the axioms of quantum theory and calculate numbers which can be compared with experimental data as long as these numbers refer to statistical averages. However, if an experiment records individual clicks of a detector it is no longer evident that the statistical properties of time series that are produced by the experiment can be described by quantum theory. Such experiments necessarily involve a fairly arbitrary (i.e. at the discretion of the experimenter) discrimination procedure to distinguish "clicks" from "no clicks" and detectors have to be calibrated "properly" [1]. This is very different from say, an experiment to observe the spectral lines of hydrogen in which it is easy to distinguish between different lines and the distances between the lines is the relevant data.

One cannot reasonably expect that some sequence of ones and zeros will yield averages that are compatible with quantum theory unless the experiment is carried out under certain very special conditions. To realize these conditions, the experimenter has to work very hard to adjust the settings of components such as mirrors, beam splitters, etc. and calibrate the detectors before the data that is being recorded exhibits features that are expected from quantum theory. For an example of an Einstein-Podolsky-Rosen-Bohm

[1] QTRF6 - Quantum Theory: Reconsideration of Foundations - 6, edited by A. Khrennikov et al., (AIP Conference Proceedings, Melville and New York, in press)

Quantum Theory: Reconsideration of Foundations 6
AIP Conf. Proc. 1508, 172-186 (2012); doi: 10.1063/1.4773129

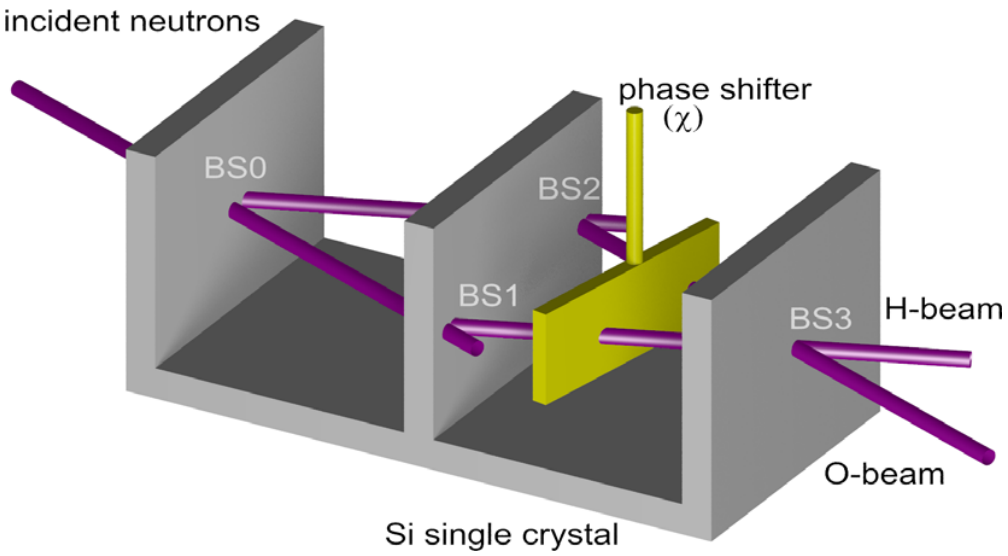

FIGURE 1. Picture of the perfect crystal neutron interferometer [4]. BS0,...,BS3: beam splitters; phase shifter: aluminum foil; neutrons that are transmitted by BS1 or BS2 leave the interferometer and do not contribute to the interference signal. Detectors count the number of neutrons in the O- and H-beam.

(EPRB) experiment in which these conditions have not been realized and the resulting data is in contradiction with the predictions of quantum theory for this experiment, see Ref. [2, 3].

From the viewpoint of quantum theory, the central issue is how it can be that experiments yield definite answers. As stated by Leggett [5], "In the final analysis, physics cannot forever refuse to give an account of how it is that we obtain definite results whenever we do a particular measurement". Although quantum theory provides a recipe to compute the frequencies for observing events it does not account for the observation of the individual events themselves, a manifestation of the quantum measurement problem [6, 7]. For a review of various approaches to the quantum measurement problem and a treatment of it within the statistical interpretation see Ref. [8].

Instead of trying to fit the observation of definite results in an axiomatic, deductive mathematical framework, we explore a very different route, rooted on the observation that empirical knowledge, and the concepts created on the basis of this knowledge, all derive from the elementary events which are registered by our senses. Clearly, this is a departure from the contemporary mode of thinking in theoretical physics, which assumes that the definite results which are observed are signatures of an underlying objective reality that is mathematical in nature. The ensuing change of paradigm lead us to explore the consequences of assuming that current scientific knowledge is built on the notion of discrete events and the relations between them, resulting in a methodology to construct simulation models which reproduce the experimental (and quantum theoretical) results of many real experiments in which the data is recorded event by event [9].

This paper shows how this change of paradigm allows us to construct a very simple simulation model which reproduces, quantitatively and without invoking quantum the-

ory, several neutron interferometry experiments. The basic device used in the neutron interferometry experiments which are covered in this paper is a Laue-type interferometer [4, 10, 11]. A large, perfect crystal of silicon is cut as shown in Fig. 1. The crystal plate BS0 acts as a beam splitter: neutrons incident from the left are transmitted with or without being refracted by this plate. Neutrons refracted by beam splitters BS1 and BS2 are directed to the third plate (BS3) which also acts as a beam splitter. Neutrons which are not refracted by beam splitters BS1 and BS2 leave the interferometer. To observe interference, the crystal planes of the different components have to be parallel to high accuracy [4] and the whole device needs to be protected from vibrations [12]. All beam splitters are assumed to have the same reflection and transmission coefficients [10]. Neutron detectors can have a very high, almost 100%, efficiency [10].

Our event-based algorithms were originally designed to simulate photon interference and EPRB photon entanglement experiments [13–17]. For many different optics experiments involving interference or correlation, the event-based corpuscular model reproduces the predictions of quantum theory and Maxwell's wave theory without solving a wave equation [17]. In this paper, we report on an extension of this approach to neutron interference experiments, demonstrating that the simulation method reproduces the results of single-neutron interferometry experiments, including experiments which, in quantum theoretical language, involve entanglement [18]. An in-depth discussion of general aspects of the event-based simulation method and of some of its applications to optics and neutron interferometry are given in Ref. [9]. Although the event-based algorithms can be given an interpretation of a realistic cause-and-effect description that is free of logical difficulties, in the absence of experiments dedicated to probe these aspects, it is difficult to decide whether or not such algorithms or modifications of them are realized by Nature.

EVENT-BASED MODEL FOR NEUTRON INTERFEROMETRY EXPERIMENTS

We now specify the model in sufficient detail such that the reader who is interested can reproduce our results.

Messenger and message: A neutron is regarded as a messenger, carrying a message. We represent a message by the two-dimensional complex-valued unit vector [18]

$$\mathbf{y} = \begin{pmatrix} e^{i\psi^{(1)}} \cos(\theta/2) \\ e^{i\psi^{(2)}} \sin(\theta/2) \end{pmatrix}. \tag{1}$$

The message Eq. (1) encodes the time of flight and the magnetic moment of the neutron. Although largely irrelevant for what follows, it may be useful to picture a messenger as a neutron carrying a clock, the hand of which rotates with angular frequency ν (to be discussed later). The clock may be used by event-based processors (to be described later), mimicking the interaction of neutrons with materials, to determine the neutron's time of flight. Imagining that the neutron is a tiny classical magnet spinning around the direction $\mathbf{m} = (\cos\phi\sin\theta, \sin\phi\sin\theta, \cos\theta)$, relative to a fixed frame of reference defined by a magnetic field, the two angles ϕ and θ suffice to specify the magnetic

moment. It is not clear whether the model of the messenger that we describe here is sufficient to reproduce the results of all possible neutron interferometry experiments but it suffices to do so for a large class of them [9].

Next, we postulate that as the messenger moves for a time T, the message changes according to

$$\mathbf{y} \leftarrow e^{i\nu T}\mathbf{y}, \tag{2}$$

where T is the time of flight, relative to the time of creation of the messenger, and ν is an angular frequency. A monochromatic beam of incident neutrons is assumed to consist of neutrons that all have the same value of ν [10]. In this paper, to simplify matters, we only consider idealized experiments with monochromatic beams of neutrons. In this case, the actual value of ν does not affect the detector counts. Event-based simulations of experiments in which the actual value(s) of ν are important, e.g. experiments which involve gravitation [10, 19–21], are left for future research.

In the event-based picture, messengers can travel along a single path only. As they travel through the interferometer (one at a time) and are detected by one of the detectors, their times of flight may be different from messenger to messenger, depending on which path they followed and the delay they experienced in the material that acts as a phase shifter. The experimentally established fact that the measured intensity depends on the position of the phase shifter is a direct proof that the messenger conveys its time of flight to the processors, hence it must have some kind of internal clock.

In the presence of a magnetic field, a magnetic moment rotates about the direction of the magnetic field according to the standard, classical equation of motion. In terms of the message, this corresponds to a rotation of $\mathbf{y}$ about the same direction. As Eq. (1) suggests, the magnetic moment is represented through the well-known Bloch-sphere representation of a spin-1/2 particle [7]. Exploiting the relation between rotations in three-dimensional space and rotations in spin-1/2 Hilbert space, in the presence of a magnetic field, the message changes according to the rule

$$\mathbf{y} \leftarrow e^{i(\sigma^x B_x+\sigma^y B_y+\sigma^z B_z)}\mathbf{y}, \tag{3}$$

where σ^x, σ^y, and σ^z are the Pauli spin-matrices and $\mathbf{B} = (B_x, B_y, B_z)$ denotes the magnetic field vector. Equation. (3) is just a convenient construct to implement rotations in three-dimensional space: The similarity to the time-evolution operator of a spin-1/2 particle is only apparent.

Particle source: The source creates messengers and initializes the message. In order to demonstrate that the class of models which we consider can produce interference without solving wave equations, we explicitly exclude the possibility that at any time there is more than one messenger passing through the interferometer, an assumption which is often made in the discussion of neutron interferometry experiments [22]. In the simulation, it is trivial to realize this condition: except for the first particle, the source creates a new particle only after the previous particle has been detected. It is also straightforward to let the source produce particles with specific properties. For instance, a fully coherent spin-polarized beam is simulated by generating messengers with the message given by Eq. (1) where $\psi^{(1)}$, $\psi^{(2)}$, and θ are the same for all messages. Throughout this paper, the total number of particles generated by the source is denoted by N.

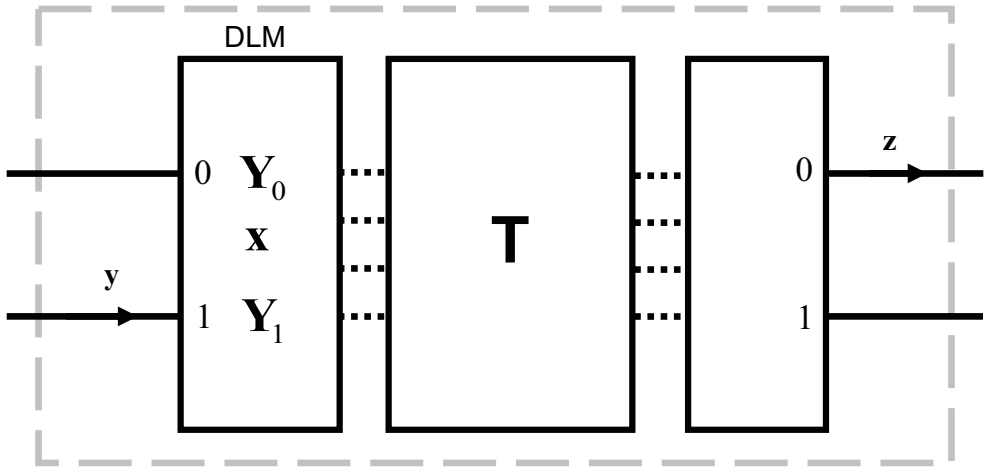

FIGURE 2. Diagram of a DLM-based processing unit that performs an event-based simulation of the beam splitters in the neutron interferometer (see Fig. 1). The processing unit consists of three stages: an input stage (DLM), a transformation stage and an output stage. The solid lines represent the input and output ports of the device. The presence of a message **y** (incident neutron) is indicated by an arrow on the corresponding port line. The DLM has storage for two real numbers (**x**) and two complex vectors $\mathbf{Y}_0$ and $\mathbf{Y}_1$ that are updated according to the rules Eqs. (5) and (4), respectively. This data is combined to yield a 4-dimensional complex-valued vector which, after transformation by a matrix **T**, is fed into the output stage which decides through which port the (modified) message **z** leaves the device. The dashed lines indicate the data flow within the unit.

Beam splitter: In Fig. 2, we show the diagram of the event-based processor that simulates the operation of a beam splitter. This processor has three stages. The input stage consists of a so-called deterministic learning machine (DLM) [13, 15, 17]. This machine is capable of learning, on the basis of the individual events, about the relative frequencies of messengers arriving on ports 0 and 1. In neutron interferometry experiments, it is assumed that at any time, at most one neutron passes through the interferometer [4, 10]. In the event-based approach, this assumption implies that the DLM receives a message on either input port 0 or 1, never on both ports simultaneously.

The arrival of a messenger at port 0 or 1 is represented by the vectors $\mathbf{v} = (1,0)$ or $\mathbf{v} = (0,1)$, respectively. A DLM that is capable of performing the desired task has an internal vector $\mathbf{x} = (x_0, x_1)$, where $x_0 + x_1 \leq 1$ and $x_k \geq 0$ for all $k = 0, 1$. In addition to the internal vector **x**, the DLM should have two sets of two registers $\mathbf{Y}_k = (Y_{k,1}, Y_{k,2})$ to store the last message **y** that arrived at port k. Thus, the DLM has storage for exactly 10 real numbers.

Upon receiving a messenger at input port k, the DLM performs the following steps: it copies the elements of message **y** in its internal register $\mathbf{Y}_k$

$$\mathbf{Y}_k \leftarrow \mathbf{y} \tag{4}$$

while leaving $\mathbf{Y}_{1-k}$ unchanged, and updates its internal vector **x** according to

$$\mathbf{x} \leftarrow \gamma\mathbf{x} + (1-\gamma)\mathbf{v}. \tag{5}$$

It is easy to show that $x_0 + x_1 \leq 1$ at all times. Each time a messenger arrives at one of the input ports, the DLM updates the values of the internal vector $\mathbf{x}$ and overwrites the values in the registers $\mathbf{Y}_k$. Thus, the machine can only store data of two messengers, not of all of them.

The parameter $0 \leq \gamma < 1$ affects the number of events the machine needs to adapt to a new situation, that is when the ratio of particles on paths 0 and 1 changes. By reducing γ, the number of events needed to adapt decreases but the accuracy with which the machine reproduces the ratio also decreases. In the limit that $\gamma = 0$, the machine learns nothing: it simply echoes the last message that it received [13, 15]. If $\gamma \to 1^-$, the machine learns slowly and reproduces accurately the ratio of particles that enter via port 0 and 1. It is in this case that the machine can be used to reproduce, event-by-event, the interference patterns that are characteristic of quantum phenomena [13, 15, 17, 18].

The second stage of the processor accepts a message from the input stage and transforms it into a new message. From the description of the DLM, it is clear that the internal registers $\mathbf{Y}_0$ and $\mathbf{Y}_1$ contain the last message that arrived on input port 0 and 1 respectively. First, this data is combined with the data of the internal vector $\mathbf{x}$, the components of which converge (after many events have been processed) to the relative frequencies with which the messengers arrive on port 0 and 1, respectively. The output message generated by the transformation stage is

$$\begin{pmatrix} Z_{0,1} \\ Z_{1,1} \\ Z_{0,2} \\ Z_{1,2} \end{pmatrix} = \begin{pmatrix} \sqrt{T} & i\sqrt{R} & 0 & 0 \\ i\sqrt{R} & \sqrt{T} & 0 & 0 \\ 0 & 0 & \sqrt{T} & i\sqrt{R} \\ 0 & 0 & i\sqrt{R} & \sqrt{T} \end{pmatrix} \begin{pmatrix} x_0^{1/2} & 0 & 0 & 0 \\ 0 & x_1^{1/2} & 0 & 0 \\ 0 & 0 & x_0^{1/2} & 0 \\ 0 & 0 & 0 & x_1^{1/2} \end{pmatrix} \begin{pmatrix} Y_{0,1} \\ Y_{1,1} \\ Y_{0,2} \\ Y_{1,2} \end{pmatrix}, \tag{6}$$

where the reflection R and transmission $T = 1 - R$ are real numbers that are considered to be parameters, to be determined from experiment. Note that in contrast to optics [17] where S- and P-polarized waves may behave differently upon reflection/transmission [23], in the case of neutrons, the first matrix in Eq. (6) (reading from left to right) treats the first and second pair of the four-dimensional vector on equal footing, in concert with the quantum theoretical treatment that yields Eqs. (13) and (14). Further note that as $x_0 + x_1 \leq 1$ at all times and $\|\mathbf{Y}_0\| = \|\mathbf{Y}_1\| = 1$, we have $|Z_{0,1}|^2 + |Z_{0,2}|^2 + |Z_{1,1}|^2 + |Z_{1,2}|^2 \leq 1$.

The output stage uses the data provided by the transformation stage to decide through which of the two ports a messenger (representing a neutron) will be sent. The rule is very simple. We compute $z = |Z_{1,1}|^2 + |Z_{1,2}|^2$ and select the output port k' by the rule

$$k' = \Theta(z - \mathscr{R}), \tag{7}$$

where $\Theta(.)$ is the unit step function and $0 \leq \mathscr{R} < 1$ is a uniform pseudo-random number (which changes with each messenger processed). From a simulation point of view, there is nothing special about using pseudo-random numbers. In fact, we use pseudo-random numbers to mimic the apparent unpredictability of the experimental data only [13, 17, 18].

The messenger leaves through either port $k' = 0$ or port $k' = 1$ carrying the message

$$\mathbf{z} = \frac{1}{\sqrt{|Z_{k',1}|^2 + |Z_{k',2}|^2}} \begin{pmatrix} Z_{k',1} \\ Z_{k',2} \end{pmatrix}, \tag{8}$$

which, for internal consistency and modularity of the event-based approach, is also a unit vector.

Detector: In the simulation model, we simply count all neutrons that leave the apparatus through the O- and H-beam. In other words, we assume that the detectors have 100% detection efficiency. Note that real neutron detectors can have efficiencies of 99% and more [12].

What makes it work?: Anticipating that the event-based processor described in this section will perform as expected, that is, produce the expected interference patterns, it may be useful to have a deeper understanding of how it can be that these patterns appear without solving a wave problem.

Let us consider BS3 in Fig. 1, the beam splitter at which, in a wave picture, the two beams join to produce interference. The event-based processor simulating a beam splitter requires two pieces of information to send out particles such that their distribution matches the wave-mechanical description of the beam splitter. First, it needs an estimate of the ratio of particle currents in the O- and H-beam, respectively. Second, it needs to have information about the time of flight along the two different paths.

The first piece of information is provided for by the internal vector $\mathbf{x}$. As explained above, through the update rule Eq. (5), for a stationary sequence of input events, $\mathbf{x} = (x_0, x_1)$ converges to the average of the number of events on input ports 0 and 1, respectively. Thus, the intensities of the waves in the two input beams are encoded in the vector $\mathbf{x}$. Note that this information is accurate only if the sequence of input events is stationary.

After one neutron arrived at port 0 and another one arrived at port 1, the second piece of information is always available in the registers $\mathbf{Y}_0$ and $\mathbf{Y}_1$. This information plays the role of the phase of the waves in the two input beams.

It is now clear that all the information (intensity and phase) is available to compute the probability for sending out particles according to the distribution that we know from wave mechanics. Indeed, in the stationary state, Eq. (6) is identical to the transformation of the wave amplitudes which we know from wave theory of a beam splitter [10, 23].

Role of the learning process: The idea that the event-based model of a beam splitter has some memory and a learning capability may seem strange enough to reject the model at first sight. However, applying the same logic to for instance Maxwell's theory of electrodynamics, one should reject this model as well. Indeed, the interaction of the electromagnetic wave and a material invariably takes a form that involves memory. This can be seen as follows. In Maxwell's theory, for electromagnetic radiation with frequency ω, the (linear part of the) interaction of the electric field $\mathbf{E}(\omega)$ and a material takes the form $\mathbf{P}(\omega) = \eta(\omega)\mathbf{E}(\omega)$ where $\mathbf{P}(\omega)$ and $\eta(\omega)$ are the polarization and dielectric susceptibility of the material, respectively [23]. Transforming this relation to

the time domain and assuming that $\mathbf{E}(t=0)=\mathbf{P}(t=0)=0$ yields [24]

$$\mathbf{P}(t)=\int_0^t \eta(t-u)\mathbf{E}(u)\,du, \tag{9}$$

where the memory kernel $\eta(t)$ is the Fourier transform of $\eta(\omega)$. Clearly, Eq. (9) shows that the response of the polarization vector to the electric field involves memory.

The analogy between Eq. (9) and the update rule Eq. (5) can be made much more explicit by assuming that $\mathbf{x}_k$ and $\mathbf{v}_k$ are the values of time-dependent vectors $\mathbf{x}(t)$ and $\mathbf{v}(t)$ sampled at regular time intervals τ. If $\mathbf{x}(t)$ allows a Taylor series expansion, we may write $\mathbf{x}_k=\mathbf{x}(\tau k)$, $\mathbf{x}_{k-1}=\mathbf{x}(\tau k)-\tau d\mathbf{x}(t)/dt|_{t=\tau k}+\mathcal{O}(\tau^2)$ such that the update rule Eq. (5) can be expressed as

$$\frac{d\mathbf{x}(t)}{dt}=-\frac{1-\gamma}{\tau\gamma}\mathbf{x}(t)+\frac{1-\gamma}{\tau\gamma}\mathbf{v}(t). \tag{10}$$

In order that Eq. (10) makes sense for $\tau\to 0$, we must have $\lim_{\tau\to 0}(1-\gamma)/\tau\gamma=\Gamma$. This requirement is trivially satisfied by putting $\gamma=1/(1+\tau\Gamma)$. Then Eq. (10) takes the form of the first-order linear differential equation

$$\frac{d\mathbf{x}(t)}{dt}=-\Gamma\mathbf{x}(t)+\Gamma\mathbf{v}(t). \tag{11}$$

Assuming $\mathbf{x}(0)=0$, the formal solution of Eq. (11) reads

$$\mathbf{x}(t)=\Gamma\int_0^t e^{-u\Gamma}\mathbf{v}(t-u)du, \tag{12}$$

which has the same structure as Eq. (9). From the derivation of Eq. (11), it follows that if we interpret τ as the time interval between two successive messages and let τ approach zero, then $\gamma=1/(1+\tau\Gamma)$ approaches one and the DLM defined by the update rule Eq. (5) "solves" the differential equation Eq. (11). Therefore, we may view Eq. (11) as a coarse-grained, continuum approximation to the event-by-event process defined by Eq. (5).

Summarizing, the general idea that objects retain some "memory" about their interaction with external agents (particles, fields,...) is not only common but even essential to some of the most successful theories of physical phenomena and can therefore not be used as an argument to dismiss a particular class of models. Furthermore, it is worth noting that Eq. (5) is not the only update rule which yields an event-based model that reproduces the averages predicted by quantum theory [13, 17]. In other words, there is nothing "unique" to Eq. (5). Whether an event-based model accounts for what is actually happening on the level of single events can only be decided by experiments that address this specific question.

NEUTRON INTERFEROMETER

A detailed quantum mechanical treatment of the interferometer depicted in Fig. 1 is given in Ref. [10, 25]. Assuming that the incident wave satisfies the Bragg condition for

scattering by the first crystal plate (BS0), the Laue-type interferometer acts as a two-path interferometer [26]. The two-path interferometer may be represented by a more abstract, theoretical model, which is similar to the one of the Mach-Zehnder interferometer for light [23], except that the latter has mirrors instead of beam splitters BS1 and BS2. In this paper, to simplify matters without giving in on the fundamental issues, we adopt an effective model for the scattering process of the neutron and the plate. We assume that the neutrons are monochromatic and satisfy the Bragg condition for scattering by the silicon plate [10]. This is not an essential simplification. In the theory of neutron interferometry, it is customary to compute the incoherent average over slight deviations from the exact Bragg condition and neutron energy [10] and the same can be done in the event-based approach as well [18]. Thus, we will characterize the beam splitters BS0,...,BS3 by effective reflection and transmission R and $T = 1 - R$, respectively.

According to quantum theory, the probabilities to observe a particle leaving the interferometer in the H- and O-beam are given by [18]

$$p_{\rm H} = R\left(T^2 + R^2 - 2RT\cos\chi\right), \tag{13}$$

$$p_{\rm O} = 2R^2T\left(1 + \cos\chi\right), \tag{14}$$

where χ is the phase shift, $R = |r|^2$ and $T = |t|^2 = 1 - R$, with t and r denoting the transmission and reflection coefficients, respectively. Note that $p_{\rm H}$ and $p_{\rm O}$ do not depend on the imaginary part of t or r, leaving only one free model parameter (e.g. R).

Interferometer: Event-by-event simulation

Using the event-based processor described earlier, it is straightforward to construct a simulation model for the interferometer shown in Fig. 1. Without any modification, we use the event-based model of a beam splitter to simulate the operation of BS0, BS1, BS2, and BS3. Neutrons that are not refracted by BS1 or BS2 leave the apparatus and do not contribute to the detection counts in the O- or H-beam [10]. During their flight from BS1 or BS2 to BS3, the neutrons pass through a metal foil which changes their time of flight [10]. Thereby it is assumed that the absorption of neutrons by the metal foil is negligible [10]. In the event-based model, when the messenger passes through the phase shifter, its message changes according to

$$\mathbf{y} \leftarrow e^{i\phi_j}\mathbf{y}, \tag{15}$$

where ϕ_j represents the change in the time of flight as the neutron passes through the metal foil on its way from BS1 to BS3 ($j = 0$) or BS2 to BS3 ($j = 1$). In neutron interferometry experiments, minute rotations of the foils about an axis perpendicular to the base plane of the interferometer induce large variations in ϕ_j [10, 27]. All the neutrons which emerge from the interferometer through the O- or H-beam contribute to the neutron count in these beams.

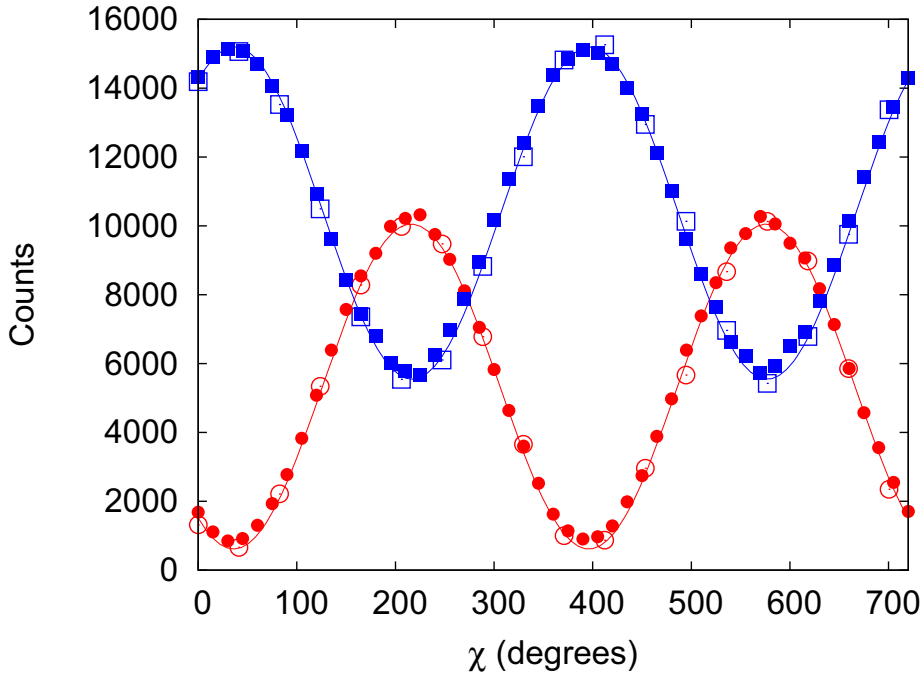

FIGURE 3. Comparison between the data (open symbols) of neutron interferometry experiments (data set rasterB1_3_1.dat kindly provided to us by Dr. H. Lemmel and Prof. H. Rauch) and the results of the discrete-event simulation (solid symbols). Open circles: counts in the O-beam; open squares: counts in the H-beam; solid circles: number of particles per sample leaving the interferometer via path 0; solid squares: number of particles per sample leaving the interferometer via path 1. Model parameters: reflection $R = 0.22$ and $\gamma = 0.7$. Lines through the data points are guides to the eye.

Simulation results

The event-by-event simulation reproduces the results of quantum theory (see Eqs. (13) and (14)) if γ approaches one [18] (data not shown). The parameter γ which controls the learning pace of the DLM-based processor can be used to account for imperfections of the neutron interferometer, thereby reducing the visibility, as observed in real neutron interferometry experiments [10]. Conclusive evidence that the event-based model reproduces the results of a single-neutron interferometry experiment comes from comparing simulation data with experimental data. In Fig. 3, we present such a comparison using experimental data provided to us by Dr. H. Lemmel and Prof. H. Rauch. The parameters R and γ and the offset in χ were varied by hand until satisfactory agreement was obtained. As shown in Fig. 3, the event-based simulation model reproduces, quantitatively, the experimental results.

VIOLATION OF A BELL INEQUALITY IN SINGLE-NEUTRON INTERFEROMETRY

The single-neutron interferometry experiment of Hasegawa *et al.* [28] demonstrates that the correlation between the spatial and spin degree of freedom of neutrons violates a Bell-CHSH inequality [29]. We take this experiment to illustrate that the event-based model reproduces this correlation by using detectors that count every neutron and without using any post-selection procedure.

A schematic picture of the single-neutron interferometry experiment is shown in Fig. 4. Incident neutrons are passing through a magnetic-prism polarizer (not shown) that produces two spatially separated beams of neutrons with their magnetic moments aligned parallel (spin up), respectively anti-parallel (spin down) with respect to the magnetic axis of the polarizer which is parallel to the guiding field **B**. The spin-up neutrons impinge on a silicon-perfect-crystal interferometer [10]. On leaving the first beam splitter, neutrons may or may not experience refraction. A mu-metal spin-turner changes the orientation of the magnetic moment from parallel to perpendicular to the guiding field **B**. The result of passing through this spin-turner is that the magnetic moment of the neutrons is rotated by $\pi/2$ ($-\pi/2$) about the y axis, depending on the path followed. Before the two paths join at the entrance plane of beam splitter BS3 a difference between the time of flights (corresponding to a phase in the wave mechanical description) along the two paths can be manipulated by a phase shifter. The neutrons which experience two refraction events when passing through the interferometer form the O-beam and are analyzed by sending them through a spin rotator and a Heusler spin analyzer. If necessary, to induce an extra spin rotation of π, a spin flipper is placed between the interferometer and the spin rotator. The neutrons that are selected by the Heusler spin analyzer are counted with a neutron detector (not shown) that has a very high efficiency ($\approx 99\%$). Note that neutrons which are not refracted by the central plate of the Si single crystal (beam splitters BS1 and BS2) leave the interferometer without being detected.

The single-neutron interferometry experiment yields the count rate $N(\alpha,\chi)$ for the spin-rotation angle α and the difference χ of the phase shifts of the two different paths in the interferometer [28]. The correlation $E(\alpha,\chi)$ is defined by [28]

$$E(\alpha,\chi)=\frac{N(\alpha,\chi)+N(\alpha+\pi,\chi+\pi)-N(\alpha+\pi,\chi)-N(\alpha,\chi+\pi)}{N(\alpha,\chi)+N(\alpha+\pi,\chi+\pi)+N(\alpha+\pi,\chi)+N(\alpha,\chi+\pi)}. \qquad (16)$$

If quantum theory describes the experiment it is expected that for the neutrons detected in the O-beam, $E(\alpha,\chi)=\cos(\alpha+\chi)$ implying $|S|=E(\alpha,\chi)-E(\alpha,\chi')+E(\alpha',\chi)+E(\alpha',\chi')>2$ for some values of α, α', χ and χ' so that the state of the neutron cannot be written as a product of the state of the spin and the phase. Experiments indeed show that $|S|>2$ [28, 30].

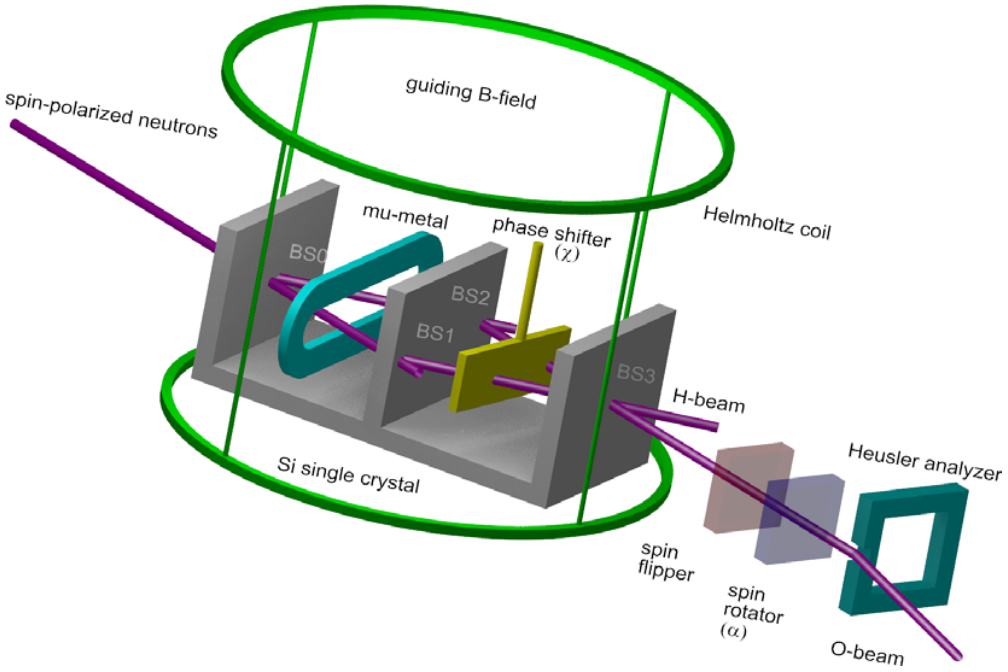

FIGURE 4. Diagram of the single-neutron interferometry experiment to test a Bell inequality violation (see also Fig. 1 in Ref. [28]).

Event-based model

A minimal, discrete event simulation model of the single-neutron interferometry experiment requires a specification of the information carried by the particles, of the algorithm that simulates the source and the interferometer components, and of the procedure to analyze the data. Most of these specifications have already been given earlier, so we only add those that correspond to components that are not present in the simple neutron interferometer shown in Fig. 1.

Mu-metal spin turner: This component rotates the magnetic moment of a neutron that follows the H-beam (O-beam) by $\pi/2$ $(-\pi/2)$ about the y axis.

Spin-rotator and spin-flipper: The spin-rotator rotates the magnetic moment of a neutron by an angle α about the x axis. The spin flipper is a spin rotator with $\alpha = \pi$.

Spin analyzer: This component selects neutrons with spin up, after which they are counted by a detector. The model of this component projects the magnetic moment of the particle on the z axis and sends the particle to the detector if the projected value exceeds a pseudo-random number $\mathscr{R}$.

Simulation results

In Fig. 5 we present simulation results for the correlation $E(\alpha, \chi)$, assuming that the experimental conditions are very close to ideal. For the ideal experiment quantum theory

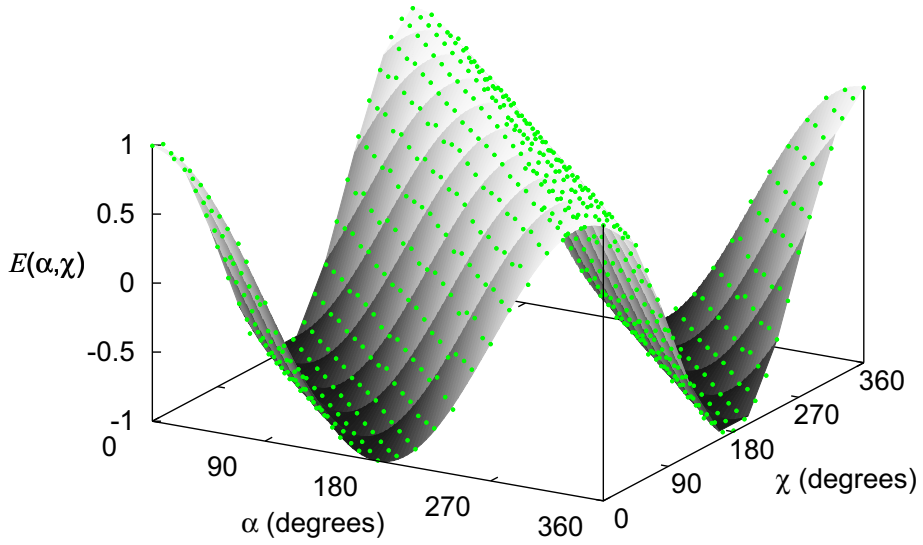

FIGURE 5. Correlation $E(\alpha,\chi)$ between spin and path degree of freedom as obtained from an event-based simulation of the experiment depicted in Fig. 4. Solid surface: $E(\alpha,\chi)=\cos(\alpha+\chi)$ predicted by quantum theory; circles: simulation data. Model parameters: $R=0.2$ and $\gamma=0.99$. For each pair (α,χ), four times 10000 particles were used to determine the four counts $N(\alpha,\chi)$, $N(\alpha+\pi,\chi+\pi)$, $N(\alpha,\chi+\pi)$ and $N(\alpha+\pi,\chi+\pi)$.

predicts that $E(\alpha,\chi)=\cos(\alpha+\chi)$. As shown by the markers in Fig. 5, disregarding the small statistical fluctuations, there is close-to-perfect agreement between the event-based simulation data and quantum theory. The laboratory experiment suffers from unavoidable imperfections, leading to a reduction and distortion of the interference fringes [28]. In the event-based approach it is trivial to incorporate mechanisms for different sources of imperfections by modifying or adding update rules. However, to reproduce the available data it is sufficient to use the parameter γ to control the deviation from the quantum theoretical result. For instance, for $\gamma=0.55$ the simulation (see Fig. 5) yields $S_{max}\equiv S(\alpha=0,\chi=\pi/4,\alpha'=\pi/2,\chi'=\pi/4)=2.05$, in excellent agreement with the value 2.052 ± 0.010 obtained in experiment [28]. For $\gamma=0.67$ the simulation yields $S_{max}=2.30$, also in excellent agreement with the value 2.291 ± 0.008 obtained in a similar, more recent experiment [30].

Discussion

An Einstein-Podolsky-Rosen-Bohm (EPRB) experiment can be used to test for violations of a Boole-Bell-type inequality [31] but not all experiments that test for violations

of a Boole-Bell-type inequality are EPRB experiments. Essential features of an EPRB (thought) experiment are that (1) a source emits pairs of particles with properties of which at least one is correlated, (2) as the particles leave the source, they no longer interact (but the correlations of their properties do not change), (3) the properties of the particles are determined by two spatially separated analyzers which do not communicate with each other and have settings that may be changed independently and randomly, (4) all particles leaving the source are analyzed and contribute to the averages and correlations. Clearly, the neutron interferometry experiment which we have discussed in this section is not an EPRB experiment. It only satisfies the fourth criterion if we disregard the neutrons that are transmitted by BS1 or BS2.

The violation of the Bell-CHSH inequality observed in the neutron interferometry experiment demonstrates that it is possible to create a correlation between the path and the magnetic moment of the neutron, although there is no direct "interaction" between the two. If we interpret the outcome of this experiment in terms of quantum theory, the observed violation of the Bell-CHSH inequality implies that it is impossible to describe the outcome of the experiment in terms of a product state of path and spin states. Hence, the system must be described by an entangled state. On the other hand, a classical, Einstein-local and causal, event-by-event process can also reproduce all the features of the entangled state. In fact, it is not a mystery that our event-based model can produce data that violates a Bell inequality. Indeed, it is well-known that contextuality (literally meaning "being dependent of the experimental measurement arrangement") can lead to violations of Bell's inequality without appealing to nonlocality or nonobjectivism [32, 33] and it is not difficult to see that the event-based model is contextual and non-Kolmogorovian.

If we pick the angle χ randomly from the same finite set of predetermined values used to produce Fig. 5, an event-based simulation with $\gamma = 0.99$ yields (within the usual statistical fluctuations) the correlation $E(\alpha,\chi) \approx (1/2)\cos(\alpha+\chi)$, which does not lead to a violation of a Bell-type inequality (data not shown). Thus, if the neutron interferometry experiment could be repeated with random choices for the position of the phase shifter (χ), and the experimental results would show a significant violation of a Bell-type inequality, the event-based model that we have presented here would be ruled out.

CONCLUSION

We have demonstrated that the event-based approach, originally introduced in Ref. [13–15] to simulate quantum optics experiments, can also be applied to neutron interferometry experiments. The result is a detailed, mystery-free, particle-only description of interference and entanglement phenomena observed in neutron interferometry experiments [10]. The statistical distributions which are observed in real experiments, usually thought to be of quantum mechanical origin, emerge from a time series of discrete events generated by causal, classical, adaptive systems.

ACKNOWLEDGMENT

We have profited from very stimulating discussions with Profs. H. Rauch and J. Summhammer. This work is partially supported by NCF, the Netherlands.

REFERENCES

1. A. Khrennikov, B. Nilsson, and S. Nordebo, *J. Phys.: Conf. Ser.* **361**, 012030 (2011).
2. G. Adenier, and A. Y. Khrennikov, *J. Phys. B: At. Mol. Opt. Phys.* **40**, 131 – 141 (2007).
3. H. De Raedt, K. Michielsen, and F. Jin, *FPP6 - Foundations of Probability and Physics 6, edited by Mauro D'Ariano, Shao-Ming Fei, Emmanuel Haven, Beatrix Hiesmayr, Gregg Jaeger, Andrei Khrennikov, Jan-Åke Larsson , (AIP Conference Proceedings , Melville and New York)* **1424**, 55 (2012), URL `http://arxiv.org/pdf/1112.2629`.
4. H. Rauch, W. Treimer, and U. Bonse, *Phys. Lett. A* **47**, 369 – 371 (1974).
5. A. Leggett, "Quantum Mechanics at the Macroscopic Level," in *The Lessons of Quantum Theory: Niels Bohr Centenary Symposium*, edited by J. de Boer, E. Dal, and O. Ulfbeck, Elsevier, Amsterdam, 1987, pp. 35 – 58.
6. D. Home, *Conceptual Foundations of Quantum Physics*, Plenum Press, New York, 1997.
7. L. E. Ballentine, *Quantum Mechanics: A Modern Development*, World Scientific, Singapore, 2003.
8. A. Allahverdyan, R. Balian, and T. Nieuwenhuizen, *arXiv:1107.2138* (2011).
9. H. De Raedt, and K. Michielsen, *Ann. Phys. (Berlin)* **524**, 393 – 410 (2012).
10. H. Rauch, and S. A. Werner, *Neutron Interferometry: Lessons in Experimental Quantum Mechanics*, Clarendon, London, 2000.
11. Y. Hasegawa, and H. Rauch, *New J. Phys.* **13**, 115010 (2011).
12. G. Kroupa, G. Bruckner, O. Bolik, M. Zawisky, M. Hainbuchner, G. Badurek, R. Buchelt, A. Schricker, and H. Rauch, *Nucl. Instrum. Methods Phys. Res. A.* **440**, 604 – 608 (2000).
13. K. De Raedt, H. De Raedt, and K. Michielsen, *Comp. Phys. Comm.* **171**, 19 – 39 (2005).
14. H. De Raedt, K. De Raedt, and K. Michielsen, *J. Phys. Soc. Jpn. Suppl.* **76**, 16 – 25 (2005).
15. H. De Raedt, K. De Raedt, and K. Michielsen, *Europhys. Lett.* **69**, 861 – 867 (2005).
16. K. De Raedt, K. Keimpema, H. De Raedt, K. Michielsen, and S. Miyashita, *Euro. Phys. J. B* **53**, 139 – 142 (2006).
17. K. Michielsen, F. Jin, and H. De Raedt, *J. Comp. Theor. Nanosci.* **8**, 1052 – 1080 (2011).
18. H. De Raedt, J. Jin, and K. Michielsen, *Quantum Matter* **1**, 1 – 21 (2012).
19. A. W. Overhauser, and R. Colella, *Phys. Rev. Lett.* **33**, 1237–1239 (1974).
20. R. Colella, A. W. Overhauser, and S. A. Werner, *Phys. Rev. Lett.* **34**, 1472–1474 (1975).
21. T. Jenke, P. Geltenbort, H. Lemmel, and H. Abele, *Nat. Phys.* **7**, 468 (2011).
22. T. Unnerstall, *Phys. Lett. A* **151**, 263 – 268 (1990).
23. M. Born, and E. Wolf, *Principles of Optics*, Pergamon, Oxford, 1964.
24. A. Taflove, and S. Hagness, *Computational Electrodynamics: The Finite-Difference Time-Domain Method*, Artech House, Boston, 2005.
25. H. Rauch, and M. Suda, *Phys. Stat. Sol. A* **25**, 495–505 (1974).
26. M. A. Horne, *Physica B+C* **137**, 260 – 265 (1986).
27. H. Lemmel, and A. G. Wagh, *Phys. Rev. A* **82**, 033626 (2010).
28. Y. Hasegawa, R. Loidl, G. Badurek, M. Baron, and H. Rauch, *Nature* **425**, 45 (2003).
29. J. S. Bell, *Speakable and Unspeakable in Quantum Mechanics*, Cambridge University Press, Cambridge, 1993.
30. H. Bartosik, J. Klepp, C. Schmitzer, S. Sponar, A. Cabello, H. Rauch, and Y. Hasegawa, *Phys. Rev. Lett.* **103**, 040403 (2009).
31. H. De Raedt, K. Hess, and K. Michielsen, *J. Comp. Theor. Nanosci.* **8**, 1011 – 1039 (2011).
32. A. Y. Khrennikov, *Contextual Approach to Quantum Formalism*, Springer, Berlin, 2009.
33. A. Khrennikov, *J. Comp. Theor. Nanosci.* **8**, 1006–1010 (2011).